Chemical Engineering Journal 172 (2011) 158–166

Contents lists available at ScienceDirect

Chemical Engineering Journal

journal homepage: www.elsevier.com/locate/cej

Evaluation of cassava peel waste as lowcost biosorbent for Ni-sorption: Equilibrium, kinetics, thermodynamics and mechanism

Alfin Kurniawan[a], Aline Natasia Kosasih[a,b], Jonathan Febrianto[a], Yi-Hsu Ju[b], Jaka Sunarso[c], Nani Indraswati[a], Suryadi Ismadji[a,*]

[a] Department of Chemical Engineering, Widya Mandala Catholic University, Kalijudan 37, Surabaya 60114, Indonesia
[b] Department of Chemical Engineering, National Taiwan University of Science and Technology, 43, Sec. 4, Keelung Rd., Taipei 10607, Taiwan
[c] Australian Research Council (ARC) Centre of Excellence for Electromaterials Science, Institute for Technology Research and Innovation, Deakin University, 221 Burwood Highway, Victoria 3125, Australia

ARTICLE INFO

Article history:
Received 1 April 2011
Received in revised form 23 May 2011
Accepted 24 May 2011

Keywords:
Cassava peel
Isotherm
Nickel
Biosorption

ABSTRACT

The feasibility of cassava peel waste for Ni-sorption is evaluated in this work. The biosorbents are characterized by Boehm titration, Fourier transform-infra red (FTIR) spectroscopy, Nitrogen sorption, scanning electron microscopy-energy dispersive X-ray (SEM-EDX) analysis (e.g. elemental mapping) and X-ray photoelectron spectroscopy (XPS). Adsorption experiments are performed in batch mode at 30 °C (303.15 K), 45 °C (318.15 K) and 60 °C (333.15 K). The performance of several temperature dependence forms of isotherm models e.g. Langmuir, Freundlich, Sips and Toth to represent the adsorption equilibrium data is evaluated and contrasted. Sips model demonstrates the best fitting with the maximum uptake capacity for Ni(II) ions of 57 mg/g (0.971 mmol/g) at pH 4.5. For kinetic data correlation, pseudo-second order model shows the best representation. The chemisorption mechanism and thermodynamics aspect are also discussed.

1. Introduction

Water pollution by heavy metals is a serious environmental problem with harmful impacts to ecological balance and living organisms, including humans due to their toxicity, accumulation in food chain and persistence nature. Nickel is one type of heavy metals generated from various industrial effluents such as metal electroplating, mining and extractive metallurgy, battery and accumulator industries, pigment as well as alloy and petroleum refinery [1]. Nickel possesses carcinogenic and mutagenic properties along with its acute and chronic effect which can cause several disorders and diseases like nausea, vomiting, skin dermatitis, infertility, apathy, chronic headache, lung, kidney, liver, intestine and heart malfunction [2]. This heavy metal is considered as hazardous substance; hence its removal from wastewater forms an essential effort in the protection of environment and water resources.

A large variety of wastewater treatment methods for nickel are available which include chemical precipitation, ion exchange, membrane filtration, coagulation and flocculation, flotation, electrochemical treatment and adsorption [3]. However, most are ineffective due to low removal efficiency and high treatment cost for low contaminant concentrations. Adsorption is known as a promising technique for this purpose due to its selectivity, high efficiency, low operational cost and minimal amount of toxic sludge. Nowadays, there are great interests to find potential and alternative adsorbents from agricultural by-products and forestry wastes [4] to overcome the limitation use of commercial adsorbents such as activated carbon for industrial applications.

Abundant amount of non-used cassava peels in Indonesia (approximately 440,800 ton peels are produced in 2009) fits this purpose and might be utilized as an effective and low cost biosorbent. Recently, the utilization of this agricultural waste as alternative adsorbent for Cu(II) removal has been studied [5]. The aim of the present study is to explore the various aspects of Ni-sorption onto cassava peel, which include its equilibrium, mechanism, kinetics and thermodynamics. The temperature dependence forms of several adsorption isotherm models are adopted to correlate adsorption equilibrium data. In our previous studies, these particular models have been successfully applied to evaluate the adsorption equilibrium data of several organic compounds onto organo-clay [6,7].

2. Materials and methods

2.1. Chemicals

$NiSO_4 \cdot 6H_2O$ (A.R. Grade; Wako Pure Chemical Industries, Ltd, Taiwan) was used as metal ion source.

* Corresponding author. Tel.: +62 313891264; fax: +62 313891267.
E-mail addresses: suryadiismadji@yahoo.com, suryadi@mail.wima.ac.id (S. Ismadji).

1385-8947/$ – see front matter © 2011 Elsevier B.V. All rights reserved.
doi:10.1016/j.cej.2011.05.083

2.2. Preparation of biosorbent

Cassava peel waste was collected from a cassava starch factory located near Surabaya, East Java, Indonesia. The collected cassava peels were washed repeatedly with tap water to remove sand and surface dirt. Subsequently, the peels were dried under the sunlight for 48 h before dried further in an oven at 100 °C for 24 h. The cassava peels were then crushed using micro-hammer mill (JANKE and KUNKEL) and sieved to certain particle sizes (125–177 μm, 177–250 μm, 250–500 μm). The final product was finally kept in airtight plastic bags for further use.

2.3. Characterizations of biosorbent

2.3.1. Boehm titration

The oxides on the surfaces of the adsorbent were analyzed by Boehm titration method [8]. The procedure is as follows: a fixed amount of cassava peel (0.5 g) was added into several conical flasks containing 50 cm^3 of 0.05 N: Na_2CO_3, $NaHCO_3$, HCl and NaOH solution. Subsequently, the flasks were placed into the thermostatic bath-shaker (Memmert UM400) and shaken at room temperature for 48 h. The mixture was then decanted and filtered through using Whattman 42 filter paper, in which 10 cm^3 of the remaining solution was titrated using 0.05 N HCl or NaOH; depending on the original solution used. The amount of acid surface groups was calculated under the assumptions that NaOH neutralizes carboxylic, phenol and lactone; Na_2CO_3 neutralizes lactone and carboxylic; $NaHCO_3$ neutralizes only carboxylic. The number of basic surface groups can be determined from the amount of HCl, which reacted with sample.

2.3.2. Fourier transform-infra red (FTIR)

The surface functional groups of adsorbent were analyzed by FTIR spectroscopy, conducted in FTIR Shimadzu 8400S using KBr disk technique. The spectra data of the sample were collected in the mid-IR wavenumber range (500–4000 cm^{-1}).

2.3.3. Nitrogen sorption

The pore structure of the adsorbent was characterized by N_2 sorption using a gas sorption analyzer (Quadrasorb SI) at 77.15 K. Prior to the adsorption analysis, the sample was degassed in a vacuum condition at 423.15 K for at least 24 h. The standard Brunauer–Emmett–Teller (BET) equation was used to calculate the specific BET surface area (S_{BET}) of the sample in the relative pressure (P/P_0) range from 0.06 to 0.3. The total pore volume of the sample was determined from the N_2 adsorption–desorption data at the highest relative pressure ($P/P_0 = 0.994$).

2.3.4. Scanning electron microscopy (SEM)

The surface morphology of the adsorbent was visualized in a JEOL JSM-6400F field emission SEM. The SEM sample was coated with a thin layer of platinum to make them electronically conductive. The sputter-coater (Eiko IB-5) was operated at 6 mA for 4 min in an argon atmosphere. The coated sample was then placed in the SEM specimen chamber and scanned at an electron acceleration voltage of 10 kV, spot size of 8, aperture of 4 and 37 mm working distance.

2.3.5. Energy dispersive X-ray (EDX) and X-ray elemental mapping

The EDX spectra and X-ray elemental mapping of the metal-loaded adsorbent were obtained using a JEOL JSM-6460 LA low vacuum analytical SEM equipped with EDX-spectrometer. Prior to the analysis, the sample was coated with carbon fiber using a custom-made carbon coater. Acquisition conditions on the SEM were 20 kV, 10 mm working distance and 30 s live time acquisition at approximately 10–15% dead time. The X-ray data of the sample were recorded and analyzed using integrated JEOL analysis station (v3.2) software.

2.3.6. X-ray photoelectron spectroscopy (XPS)

The XPS spectra of the metal-loaded adsorbent were obtained with a Kratos Axis ULTRA X-ray Photoelectron Spectrometer using monochromatic Al Kα X-ray radiation (1486.6 eV) at 150 W (15 kV, 15 mA). Survey scans were collected at binding energy range of 0–1200 eV with the pass energy adjusted to 160 eV and narrow high-resolution scans at 20 eV. Survey scans were run with 1.0 eV steps and 100 ms dwell time while narrow high-resolution scans were run with 0.05 eV steps and 250 ms dwell time. Base pressure in the analysis chamber was 1.0×10^{-9} Torr and during sample analysis was 1.0×10^{-8} Torr.

2.4. Biosorption experiments

The stock solution of $NiSO_4{\cdot}6H_2O$ at initial concentration of 200 mg/L was used as synthetic effluent. This solution was prepared by dissolving a fixed amount of $NiSO_4{\cdot}6H_2O$ into 1 L deionized water. The biosorption equilibrium experiments were conducted by adding various mass of adsorbents (0.1–10 g) into several conical flasks containing 100 mL of metal solution. Subsequently, the flasks were placed in a thermostat orbital shaker incubator LM-570 and heated from room temperature to the desirable operating temperature (30 °C, 45 °C, 60 °C). The shaker was then set to rotate at 200 rpm within 2–3 h to reach equilibrium. The metal solution was then centrifuged (Hettich Zentrifugen EBA-20) at 4000 rpm for 5 min to remove solid particles. The residual Ni-metal concentration in solution was analyzed using a flame atomic absorption spectrophotometer (Shimadzu AA6200) at $\lambda = 232.7$ nm.

For biosorption kinetics, the experiments were carried out as follows: 100 mL of metal solution at initial concentration of 200 mg/L was mixed with 0.5 g of adsorbent with certain particle size in several conical flasks. The flasks were then placed in an orbital shaker incubator and shaken at 60 °C and 200 rpm for certain period of time. During the experiments, at certain interval of time, 10 mL of metal solution was taken from the flasks, centrifuged and analyzed its residual nickel metal concentration. The effect of pH was also studied at pH range of 1.0–9.0. To adjust pH, an appropriate amount of 0.1 N HCl or NaOH solutions was added. All experiments were carried out in triplicate with their averages used as the result.

The uptake capacity of cassava peel, in the unit concentration of mmol/g can be calculated using following mass balance equation:

$$q_e = \frac{(C_0 - C_e)}{m} \times V \quad (1)$$

where q_e is the amount of metal uptake at equilibrium condition (mmol/g), C_0 and C_e is a symbol represented the initial and equilibrium concentration of metal ions in solution (mmol/L), m is the biosorbent dose (g) and V is the volume of metal solution (L).

3. Results and discussion

3.1. Characterizations of pristine cassava peel

The surface morphology of cassava peel is depicted in Fig. 1. Fig. 1 features the non-porous, heterogeneous and complex nature of cassava peel surface. The N_2 sorption analysis (Fig. 2) is consistent with the SEM result. The specific BET surface area (S_{BET}) of this peel is 3.72 m^2/g with N_2 sorption capacity of 20.2 cm^3/g (STP). Low S_{BET} value is likely due to the low porosity on the material surface [9–11]. The presence of surface oxides in cassava peel can be detected by Boehm titration. The cassava peel surface is mainly

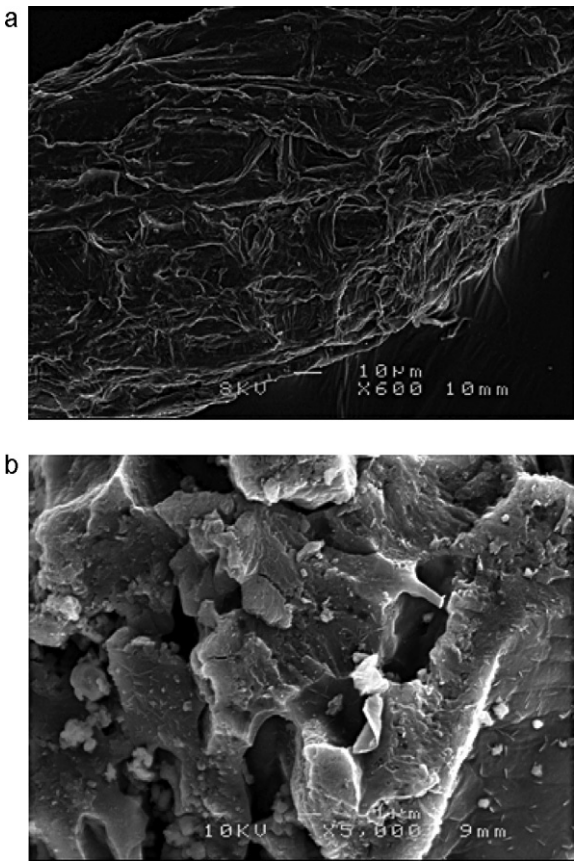

Fig. 1. SEM micrographs of cassava peel at two magnifications (a) 600× and (b) 5000×.

occupied by acidic groups (0.526 meq/g) and small amount of basic groups (0.108 meq/g).

3.2. Characterizations of Ni-loaded cassava peel

3.2.1. FTIR spectroscopy

FTIR can be used to collect information regarding the vibrational frequency changes of functional groups, which are involved during sorption process. Fig. 3 presents the FTIR spectra of both pristine and Ni-loaded cassava peel for direct comparison. Fig. 3 demonstrates that cassava peel exhibits heterogeneous and complex surface with various functional groups appearing at certain wavenumber (Table 1). The alteration of several functional groups in pristine cassava peel after metal sorption was evidenced.

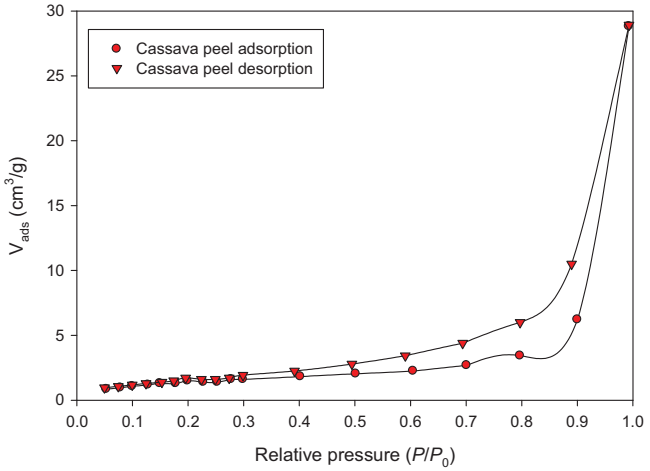

Fig. 2. N_2 adsorption–desorption isotherm of cassava peel at 77 K.

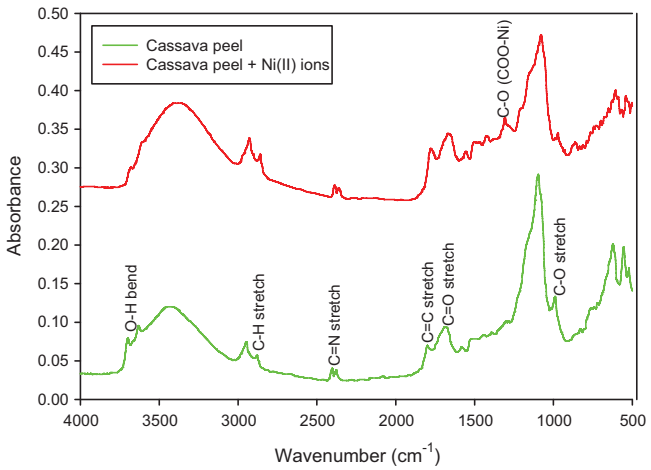

Fig. 3. FTIR spectra of pristine and Ni-loaded cassava peel.

The FTIR spectra of Ni-loaded cassava peel reveal that the alteration of absorption peaks (3620, 1340 and 942 cm^{-1}) occurs after metal sorption. The peak observed at 3620 cm^{-1}; corresponds to O–H stretch of hydroxyl groups in the lignocellulosic structure disappears (after sorption). Modification of another peak (at 942 cm^{-1} associated with the decrease of peak energy for O–H bend in carboxylic acid) is also observed due to their involvement during Ni-sorption. Moreover, the existence of new peak is also noticed at 1340 cm^{-1}; representing C–O stretch of metal–carboxylate (COO–M) groups. Overall, change in the surface functional groups of the adsorbents is mainly observed in hydroxyl and carboxyl groups; denoting that their deprotonated forms (hydroxylate and carboxylate anions) are the adsorption sites for Ni(II) [12,13].

3.2.2. Energy dispersive X-ray (EDX), X-ray elemental mapping and X-ray photo electron spectroscopy (XPS) analyses

The presence of heavy metal after sorption can be detected by analyzing the adsorbent surface using SEM-EDX, X-ray elemental mapping and XPS analyses. EDX is an analytical technique to identify the element presence on the material surface based on their characteristic X-ray energy. This technique is normally coupled with SEM analysis to gain more complete result.

The SEM-EDX spectra of Ni-loaded cassava peel are given in Fig. 4. In Fig. 4, Ni(II) ions' presence can be detected from the Ni–L and Ni–K peaks, which appear in the binding energy range of 0.85–0.87 keV and 7.5–8.3 keV, respectively. The X-ray elemental

Table 1
Functional groups of pristine and Ni-loaded cassava peel.

Functional group	Wavenumber (cm^{-1})	
	Pristine	Ni-loaded
O–H bend (carboxylic acids)	942	940
C–O stretch of –OCH_3 groups (lignocelluloses compound)	1050	1052
C–O stretch of metal–carboxylate complex (COO–Ni)	–	1340
C–C stretch (aromatics structure)	1515	1514
C=O stretch (asymmetric COO)	1636	1637
–C=C– stretch (alkenes)	1764	1762
C≡N stretch (nitrile groups)	2378	2377
C–H stretch (alkanes)	2847	2846
C–H stretch (methylene groups)	2941	2943
O–H stretch (lignocelluloses structure)	3602	–

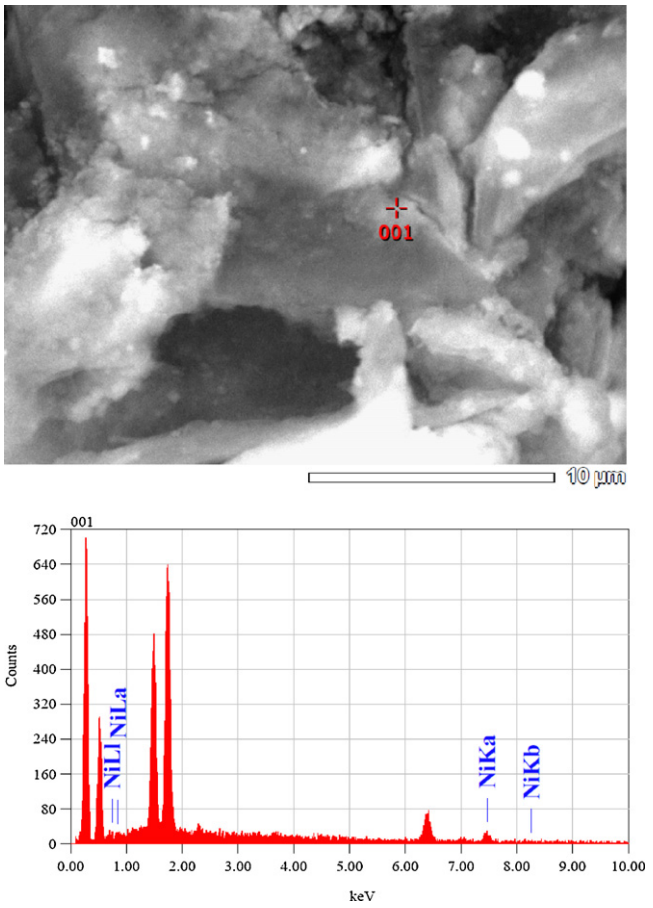

Fig. 4. SEM-EDX spectra of Ni-loaded cassava peel.

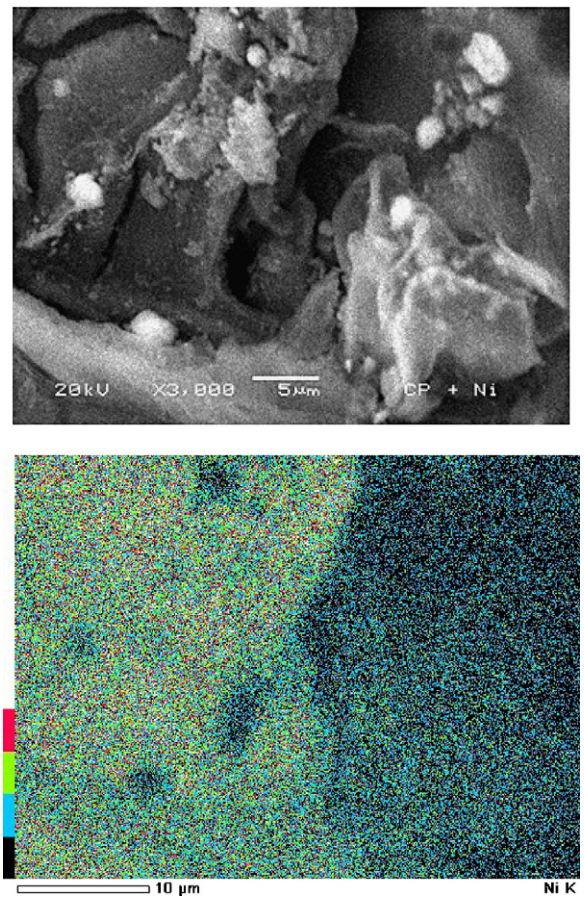

Fig. 5. SEM and X-ray elemental mapping of Ni-loaded cassava peel.

mapping is also performed to measure qualitatively the distribution of metal ions on the adsorbent surface (Fig. 5). In Fig. 5, nickel metal is represented by the bright region. The XPS spectroscopy of Ni-loaded cassava peel is recorded to gain insight into metal–surface interaction in the sorption study. Fig. 6 displays the XPS spectra of Ni-loaded cassava peel. In this figure, the presence of Ni(II) ions is verified from the assignment of Ni $2p_{3/2}$ XPS spectra, which appear at binding energy of 854.6 eV; representing Ni^{2+} in the oxide state.

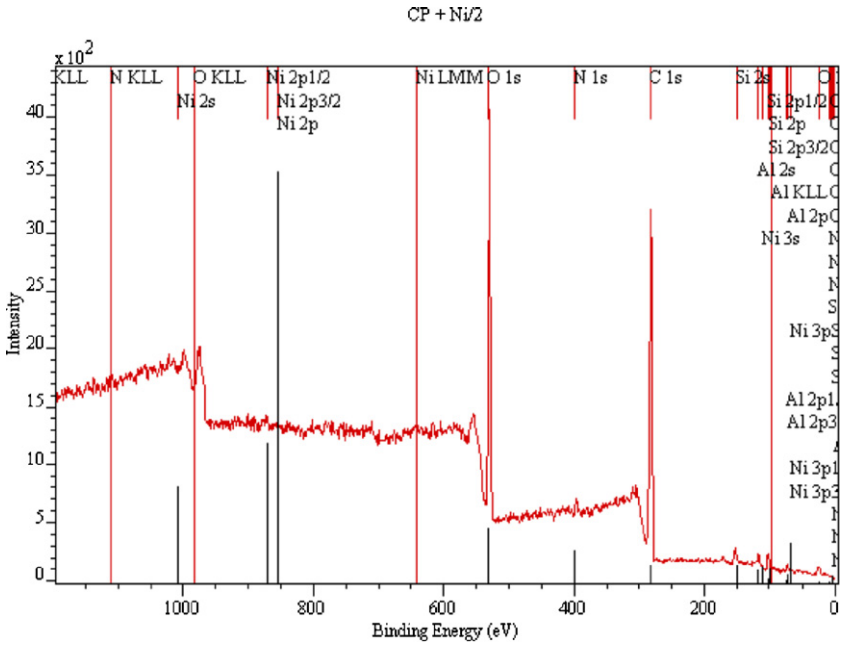

Fig. 6. XPS spectra of Ni-loaded cassava peel.

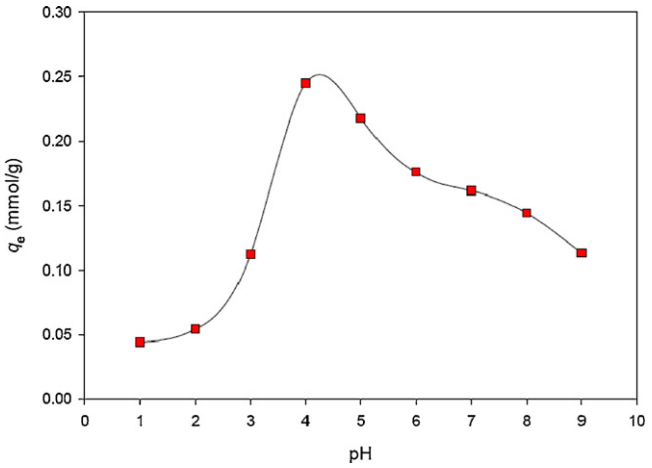

Fig. 7. Effect of pH on the Ni(II) ions equilibrium uptake (C_0 = 200 mg/L, biosorbent mass = 1.5 g, T = 45 °C).

3.3. Effect of pH

The pH is a key factor that should be considered in the sorption since it substantially affects the mechanism of metal ion uptake. The effect of pH on the Ni(II) ion uptake at equilibrium was studied by varying pH from 1 to 9. Fig. 7 shows that the amount of Ni(II) ion uptake increases steadily by increasing pH from 1 to 4 and reach its maximum at pH 4.5. At higher pH, the amount of Ni(II) adsorbed is less compared to that at pH 4.5. This phenomenon might be caused by the formation of metal hydroxide [$Ni(OH)_2$], which takes place at alkali pH range (pH > 7). The formation of $Ni(OH)_2$ reduces the concentration of Ni(II) ions in the solution; hence the percentage removal of Ni(II) by cassava peel also decreases. For this reason, pH 4.5 was selected during metal biosorption experiments and serves also as optimum value for Ni(II) removal.

Low nickel uptake in acidic solution might be due to the competition between Ni(II) ions and H_3O^+ ions for the adsorption sites, which reduced the amount of Ni(II) uptake. The presence of H_3O^+ ions also retards the Ni-sorption due to repulsion force between protonated adsorbent surface and metal cations. This phenomenon can be explained on the basis of carboxylic groups (R–COOH) being protonated by H_3O^+ ions as follows:

$$\text{R–COOH} + \text{H}_3\text{O}^+ \rightarrow \text{R–COOH}_2{}^+ + \text{H}_2\text{O} \quad (2)$$

As the pH increase, the concentration of H_3O^+ ions in metal solution decreases and the repulsion between adsorbent and adsorbate also weakens; resulting in the increase amount of adsorbed metal ions (onto the solid surface). Increasing pH also exposes more negatively charged ligands such as carboxylate anions ($R–COO^-$) on the adsorbent surface due to the dissociation of carboxylic at pH range of 3.5–5.5 [14], leading to the electrostatic attraction of Ni(II) ions onto these groups.

3.4. Chemisorption of Ni(II) ions onto cassava peel surface

The chemisorption mechanism of Ni(II) ions onto cassava peel surface was proposed in this study using molecular simulation by ChemDraw software package. Some information about the surface chemistry characterization of the adsorbents, for example the alteration of functional groups can be used as evidences in proposing biosorption mechanism. The Ni-chemisorption mechanism onto cassava peel surface and the molecular model of Ni–carboxylate complex is illustrated in Fig. 8.

In Fig. 8, it can be seen that Ni(II) ions were bound into carboxylate groups in the lignocellulosic structure of cassava peel by creating ionic forces with carboxylic oxygen atoms. These oxygen atoms exhibited negative charge in their structure as a result of the dissociation of carboxylic groups. The negatively charged oxygen atom in carboxylate anions will coordinate with nickel cations, resulting in the formation of metal–carboxylate complexes (COO–Ni) on the cassava peel surface.

The presence of metal–carboxylate complex could be also indicated from the peak at 1340 cm^{-1}, which assigned to C–O stretch of COO–Ni groups. Other phenomena were also observed during the formation of COO–Ni complex, relating to the disappearance of O–H stretch at 3600 cm^{-1} and reduction of peak energy for O–H bend at 940 cm^{-1}. This statement was in agreement with FTIR results as shown in Fig. 3.

In addition, the coordination type of metal–carboxylate complexes can also be determined by examining the vibrational modes of ν_{asym} (COO^-) and ν_{sym} (COO^-) in the wavenumber region of 1300–1750 cm^{-1}. As reported by Papageorgiou et al. [15] that the unidentate coordination of metal–carboxylate complex occurs where the difference ($\Delta\nu$) between ν_{asym} (COO^-) and ν_{sym} (COO^-) is larger than 200 cm^{-1}. In this study, the $\Delta\nu$ (COO^-) value was 297 cm^{-1}, suggested the formation of Ni–carboxylate complex through unidentate chelating coordination.

3.5. Biosorption isotherms

Biosorption isotherm is vital information from the view of practical design and operation of the sorption system as it describes the distribution of adsorbates among solid and liquid phases at equilibrium. In this work, several temperature dependence forms of isotherm models (Langmuir, Freundlich, Sips and Toth) were used to represent adsorption equilibrium data. The Langmuir model can be expressed as follows:

$$q_e = q_m \frac{K_L(T) \times C_e}{1 + K_L(T) \times C_e} \quad (3)$$

where q_m is the Langmuir based maximum adsorption capacity for particular adsorbent (mmol/g) and K_L is Langmuir parameter that defined as affinity constant at equilibrium (L/mmol). The temperature dependence form of q_m parameter, which proposed by Dubinin–Radushkevich and K_L is given as follows [16,17]:

$$q_m = q_0 \exp(\delta(T - T_0)) \quad (4)$$

$$K_L(T) = K_0 \exp\left(\frac{Q_{ads}}{RT}\right) \quad (5)$$

where q_0 is the maximum uptake capacity of adsorbate at reference temperature T_0 (298.15 K), δ is a parameter representing thermal expansion coefficient of adsorbate (K^{-1}), Q_{ads} is heat of adsorption (kJ/mol), R is the universal gas constant (8.314 J mol^{-1} K^{-1}) and K_0 is the adsorption affinity at reference temperature T_0 (L/mmol). The essential characteristic of Langmuir model can be expressed by dimensionless constant called equilibrium parameter, R_L, which defined as:

$$R_L = \frac{1}{1 + K_L C_0} \quad (6)$$

The value of R_L indicates various characteristics of adsorption isotherm to be irreversible (R_L = 0), linear (R_L = 1), unfavorable (R_L > 1) and favorable (0 < R_L < 1).

The second adsorption model is Freundlich. This model was proposed by Freundlich (1932) assuming that the adsorbent surface is heterogeneous with uneven distribution of adsorption heat and affinity over the solid surface. Although Freundlich model has widely applied in many sorption studies, it has a limitation in correlating equilibrium data at wide concentration range since this isotherm does not have a proper Henry law limit at low

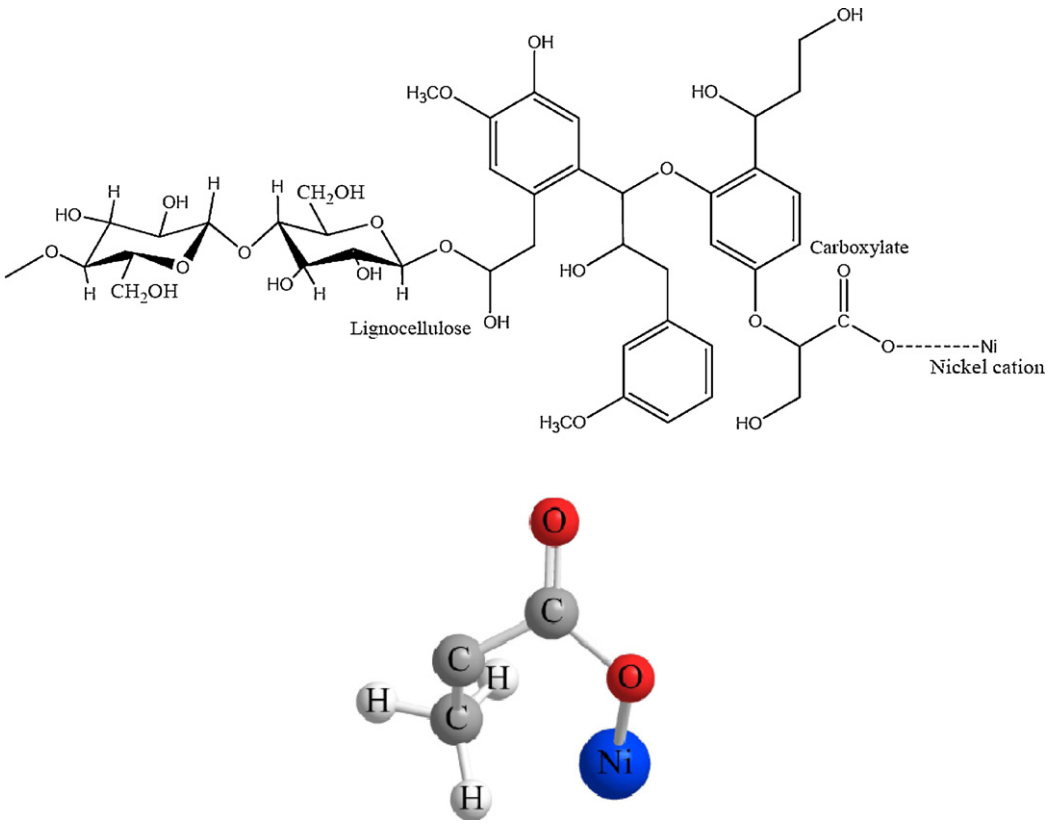

Fig. 8. Ni-chemisorption mechanism and the model of Ni–carboxylate complex.

concentration and does not have a saturation limit at high-end concentration. The Freundlich model has the following form:

$$q_e = K_F(T) \times C_e^{1/n} \tag{7}$$

where n and K_F are the Freundlich parameters which represent the system heterogeneity and adsorption capacity [(mmol/g)(mmol/L)$^{-n}$], respectively. The parameter K_F and n can be expressed as the temperature dependence form as follows [16]:

$$K_F = K_{F_0} \exp\left(-\frac{\alpha RT}{A_0}\right) \tag{8}$$

$$\frac{1}{n} = \frac{RT}{A_0} \tag{9}$$

The third adsorption model is Sips. Sips (1948) proposed an empirical equation describing adsorption behavior in heterogeneous system which has similar form to Langmuir model:

$$q_e = q_m \left(\frac{(C_e \times K_S(T))^{1/n}}{1 + (C_e \times K_S(T))^{1/n}}\right) \tag{10}$$

The temperature dependence forms of Sips parameter are [16]:

$$K_S = K_{S_0} \exp\left[\frac{Q_{ads}}{RT_0((T/T_0) - 1)}\right] \tag{11}$$

$$n = \frac{1}{(1/n_0) + \sigma(1 - (T/T_0))} \tag{12}$$

where K_{S_0} and n_0 is the adsorption affinity and the system heterogeneity parameter at reference temperature T_0 (298.15 K), respectively and σ is a constant parameter.

The last adsorption model is Toth. The Toth model is one of the most popular three-parameter adsorption equations used in predicting adsorption phenomena in heterogeneous system due to its capability to overcome the drawback of Sips and Freundlich model. The Toth model has the form:

$$q_e = q_m \frac{b_T(T) \times C_e}{(1 + (b_T(T) \times C_e)^t)^{1/t}} \tag{13}$$

Here t and b_T are the Toth parameter characterizing the system heterogeneity and the biosorption affinity (L/mmol), which is specific for adsorbent–adsorbate system. The parameter b_T and t in Toth model can be expressed as temperature function [16]:

$$b_T = b_0 \exp\left[\frac{Q_{ads}}{RT_0}\left(\frac{T}{T_0 - 1}\right)\right] \tag{14}$$

$$t = t_0 + \sigma\left(1 - \frac{T}{T_0}\right) \tag{15}$$

where b_0 and t_0 are the adsorption affinity and t parameter at reference temperature T_0 (298.15 K) and σ is a constant parameter.

The Ni-sorption equilibrium data at three different temperatures e.g. 30 °C (303.15 K), 45 °C (318.15 K) and 60 °C (333.15 K) and the fitting of isotherm models are shown in Fig. 9. The isotherm parameters were calculated by nonlinear regression method (Table 2). Fig. 9 shows that all models could fit the adsorption equilibrium data well ($R^2 > 0.998$), however, to assess the applicability and suitability of the models in correlating experimental data, the physical meaning of each parameter should be examined.

The parameter q_0, which represents the maximum uptake capacity of adsorbent at temperature T_0, refers to the complete monolayer coverage. Table 2 demonstrates that the values of q_0 parameter for Langmuir, Sips and Toth models are similar. These parameter values correspond to the Ni(II) ion uptake around 57 mg/g. Therefore, the value of q_0 parameter in Langmuir, Sips and Toth is reasonable and consistent. For comparison purpose, the maximum biosorption capacity of several adsorbents for Ni(II)

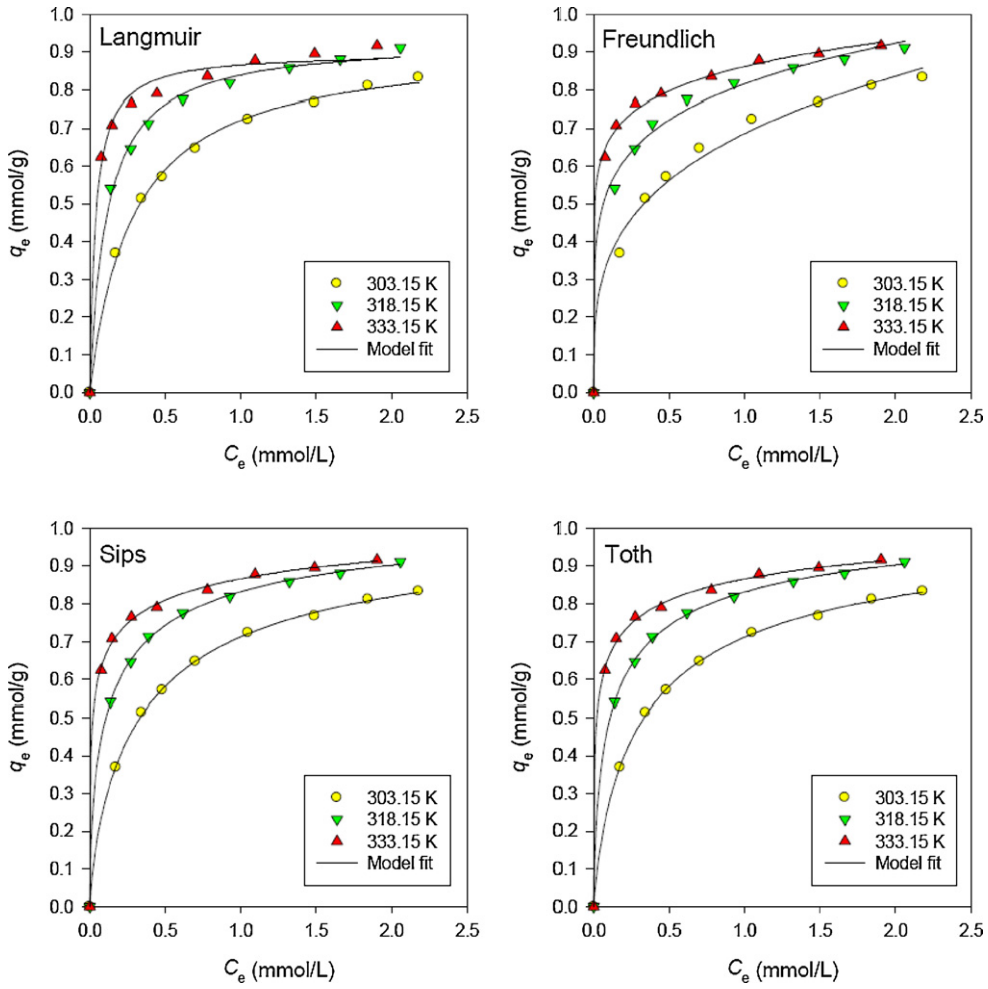

Fig. 9. Ni-sorption equilibrium data and the fitting of temperature dependence forms of isotherm models (C_0 = 200 mg/L, particle size = 125–177 μm, pH = 4.5).

ion removal is also given in Table 3. The maximum uptake capacity (indicated by K_{F_0}) from Freundlich model is significantly larger (192.5 mg/g) than that from other models. For non-treated biosorbent, the obtained maximum uptake capacity value is not possible; hence this model is not discussed further.

Table 2
The fitted temperature dependence parameters of isotherm models for Ni-sorption onto cassava peel.

Isotherm model	Parameter	Value	R^2
Langmuir	q_0 (mmol/g)	0.972	0.9982
	δ (1/K)	0.00628	
	K_0 (L/mmol)	2.614×10^{-6}	
	Q_{ads} (kJ/mol)	40.17	
Freundlich	K_{F_0} [(mmol/g)(mmol/L)$^{-n}$]	3.279	0.9991
	α/A_0 (mol/J)	3.416×10^{-4}	
Sips	q_0 (mmol/g)	0.989	0.9987
	δ (1/K)	0.00607	
	K_{S_0} (L/mmol)	2.246	
	Q_{ads} (kJ/mol)	41.03	
	n_0	1.159	
	σ	4.637	
Toth	q_0 (mmol/g)	0.981	0.9989
	δ (1/K)	0.00619	
	b_0 (L/mmol)	1.835	
	Q_{ads} (kJ/mol)	40.64	
	t_0	3.129	
	σ	14.473	

Further verification was performed onto K_0, K_{S_0} and b_0 parameters, which is defined as adsorption affinity. K_0, in particular, this parameter measures how strong the interaction force between adsorbate molecule and adsorbent surface. Both adsorption affinities of Sips and Toth models are comparable to values reported for other sorption systems, however the fitting value of parameter K_0 in Langmuir model is considerably low and not consistent with the value reported on most sorption systems.

Table 3
The maximum sorption capacity of various adsorbents for Ni(II) removal.

Adsorbent	Operating condition		q_m (mg/g)	Reference
	pH	T (K)		
Cashew nut shell	5	303.15	18.87	[22]
Orange peel	5.5	303.15	9.82	[12]
OPAA – modified orange peel	5.5	303.15	162.6	[12]
Pomegranate peel	–	318.15	69.4	[23]
Sargassum muticum	3	293.15	70.0	[24]
Gracilaria caudata	5	293.15	45	[24]
Pine bark	8	–	12.15	[25]
H_3PO_4 – treated rice bran	6	303.15	102	[26]
Acid – treated peepal leaf	7	–	6.35	[27]
Barley straw	4.85	296.15	35.8	[28]
Moringa oleifera bark	6	323.15	30.38	[13]
Cassava peel	4.5	–	57	This study

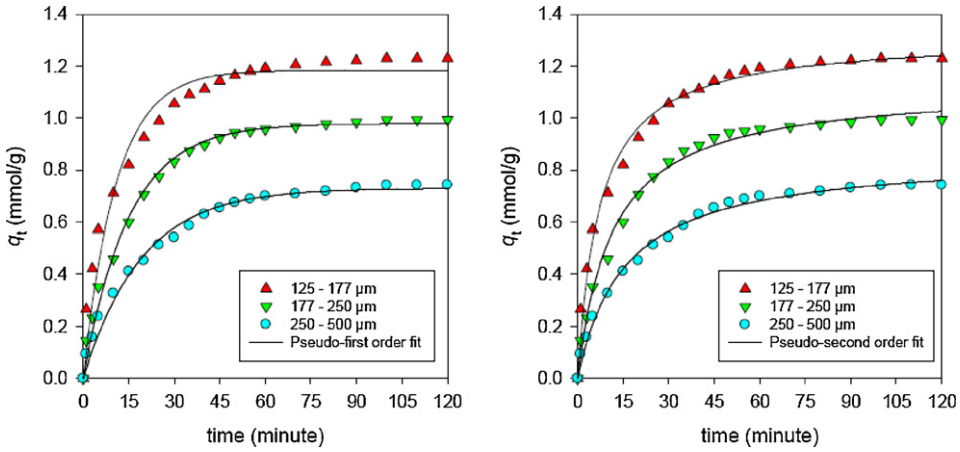

Fig. 10. Ni-biosorption kinetic data and the fitting of kinetic models (C_0 = 200 mg/L, T = 60 °C, biosorbent mass = 0.5 g, pH = 4.5).

The last verification of the physical meaning of the remaining isotherm models (Sips and Toth) is on the n_0 or t_0 parameter, which represents the heterogeneity of the system. If its value deviates away from unity, the sorption system is considered more heterogeneous. The value of t_0 in Toth model is usually less than unity while the n_0 parameter in Sips model is greater than unity [16]. Sips model provide reasonable parameter value while Toth model gives incorrect value (Table 2).

Thus, Sips model provides the best representation on the experimental data. The chemisorption nature of Ni-sorption is also supported by Sips model on which the Q_{ads} value lies between 40 and 400 kJ/mol.

3.6. Biosorption kinetics

In order to investigate the potential rate-controlling step involved, two kinetic models namely pseudo-first order and pseudo-second order were used to evaluate kinetic data. The pseudo-first order, which is also known as Lagergren equation can be expressed as follows [18]:

$$q_t = q_e(1 - \exp(-k_1 t)) \tag{16}$$

while the pseudo-second order model [19] has the form as described in Eq. (17):

$$q_t = \frac{k_2 q_e^2 t}{1 + k_2 q_e t} \tag{17}$$

where q_t and q_e is the amount of Ni(II) ions adsorbed at time t and equilibrium condition (mmol/g), respectively. The rate constant of k_1 (1/min) and k_2 (g/(mmol min)) was attributed to pseudo-first order and pseudo-second order model, respectively and t is time (min). The plot of the experimental data and the model fitting are illustrated in Fig. 10. The kinetic parameters obtained by non-linear regression method are tabulated in Table 4.

Table 4 shows that particle size has significant effect to the rate constant (k) and nickel equilibrium uptake (q_e). Smaller particle size increases the rate constant and nickel equilibrium uptake to the extent that the equilibrium condition is achieved faster. Smaller particles also provide larger surface area and more available binding sites for Ni(II) ions onto their surface; leading to faster metal ion uptake.

Comparing the correlation coefficient (R^2) value, the pseudo-second order is better than the pseudo-first order model. In addition, the q_e parameter in pseudo-second order model provides closer value to the experimental results. These facts suggest that the potential rate-controlling step in Ni-sorption is chemisorption involving cation exchange reaction between adsorbate and adsorbent, surface complexation, coordination and/or chelation.

3.7. Thermodynamics aspects

Thermodynamic parameters relevant to the sorption process are the change in standard Gibb's free energy (ΔG°), entropy (ΔS°) and enthalpy (ΔH°); which can be determined using following equations:

$$\Delta G^\circ = -RT \ln K_D \tag{18}$$

$$\ln K_D = -\frac{\Delta H^\circ}{RT} + \frac{\Delta S^\circ}{R} \tag{19}$$

where R is the universal gas constant (8.314 J mol^{-1} K^{-1}), T is the temperature (K) and K_D is the thermodynamic distribution coefficient, defined as:

$$K_D = \frac{C_a}{C_e} \tag{20}$$

where C_a is the equilibrium metal concentration on the solid surface (mmol/L) and C_e is the equilibrium metal concentration in the bulk solution (mmol/L). The enthalpy and entropy change can be calculated from the slope and intercept of Van't Hoff plot of ln K_D vs $1/T$ (Fig. 11). The calculated thermodynamic parameters are given in Table 5.

Negative values of ΔG° are displayed in Table 5 at all temperatures, which indicate the favorability and spontaneous nature of

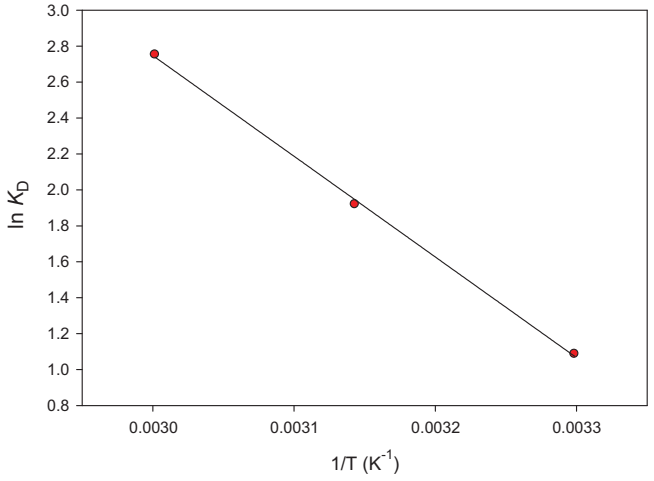

Fig. 11. Thermodynamic plot of ln K_D versus $1/T$ of Ni-sorption onto cassava peel.

Table 4
The fitted parameters of kinetic models for Ni-sorption onto cassava peel.

Particle size (μm)	q_e exp (mmol/g)	Kinetic model					
		Pseudo-first order			Pseudo-second order		
		k_1	q_e	R^2	k_2	q_e	R^2
125–177	1.2304	0.0920	1.1840	0.9629	0.1039	1.2351	0.9903
177–250	0.9933	0.0665	0.9787	0.9909	0.0772	1.0147	0.9926
250–500	0.7418	0.0524	0.7297	0.9858	0.0754	0.7475	0.9936

Table 5
Thermodynamic parameters of Ni-sorption onto cassava peel.

T (K)	ΔG° (kJ/mol)	ΔH° (kJ/mol)	ΔS° (kJ/mol K)	R^2
303.15	−2.738	46.584	0.162	0.9992
318.15	−5.077			
333.15	−7.623			

Ni-sorption process. As the temperature increases, the ΔG° value becomes more negative which implies that higher temperature favors Ni-sorption. The positive value of ΔH° denotes the endothermic nature of this sorption process and acts as another evidence of its chemisorption nature since ΔH° value lies between 20.9 and 418.4 kJ/mol [20]. This observation is also supported by the increased amount of adsorbed nickel at higher temperature. On the other hand, the positive value of ΔS° denotes the internal structural changes of the cassava peel due to the intercalation of Ni(II) ions and the increase in the disorder degree at solid–solution interface due to the desolvation in bulk solution during metal sorption process [21].

4. Conclusions

This work evaluates various aspects of Ni-sorption onto cassava peel waste. Characterizations of adsorbent are conducted to analyze the surface morphology and surface chemistry of cassava peel before and after metal sorption. To assess the feasibility of cassava peel waste to remove Ni(II) ions, the biosorption experiments are carried out in batch mode. The maximum uptake capacity (q_m) of cassava peel is 57 mg/g at pH 4.5. The Sips model provides the best representation for adsorption equilibrium data. In kinetic data correlation, the pseudo-second order is superior to the pseudo-first order model. The Ni-sorption mechanism is also discussed from molecular point of view. Lastly, thermodynamic results indicate the endothermic ($\Delta H^\circ > 0$), spontaneous ($\Delta G^\circ < 0$) and irreversible ($\Delta S^\circ > 0$) natures of Ni-sorption onto cassava peel.

References

[1] M. Monier, D.M. Ayad, Y. Wei, A.A. Sarhan, Adsorption of Cu(II), Co(II) and Ni(II) ions by modified magnetic chitosan chelating resin, J. Hazard. Mater. 177 (2010) 962–970.
[2] R.P. Beliles, The lesser metals, in: F.W. Oehme (Ed.), Toxicity in Heavy Metals in the Environment, Part 2, Marcel Dekker, New York, 1978.
[3] F. Fu, Q. Wang, Removal of heavy metal ions from wastewaters: a review, J. Environ. Manage. 92 (2011) 407–418.
[4] A. Bhatnagar, M. Sillanpaa, Utilization of agro-industrial and municipal waste materials as potential adsorbents for water treatment – a review, Chem. Eng. J. 157 (2010) 277–296.
[5] A.N. Kosasih, J. Febrianto, J. Sunarso, Y.-H. Ju, N. Indraswati, S. Ismadji, Sequestering of Cu(II) from aqueous solution using cassava peel (*Manihot esculenta*), J. Hazard. Mater. 180 (2010) 366–374.
[6] A.K. Rahardjo, M.J.J. Susanto, A. Kurniawan, N. Indraswati, S. Ismadji, Modified Ponorogo bentonite for the removal of ampicillin from wastewater, J. Hazard. Mater. 190 (2011) 1001–1008.
[7] F.P. Yesi, H.-Y. Sisnandy, F.E. Ju, S. Soetaredjo, Ismadji, Adsorption of acid blue 129 from aqueous solutions onto raw and surfactant modified bentonite: the application of temperature dependent form of adsorption isotherms, Adsorpt. Sci. Technol. 28 (2010) 847–868.
[8] H.P. Boehm, Surface oxides on carbon and their analysis: a critical assessment, Carbon 40 (2002) 145–149.
[9] L.M. He, B.M. Tebo, Surface charge properties of and Cu(II) adsorption by spores of the marine Bacillus sp. Strain SG-1, Appl. Environ. Microbiol. 64 (1998) 1123–1129.
[10] N. Fiol, I. Villaescusa, M. Martinez, N. Miralles, J. Poch, J. Serarols, Sorption of Pb(II), Ni(II), Cu(II) and Cd(II) from aqueous solution by olive stone waste, Sep. Purif. Technol. 50 (2006) 132–140.
[11] S.K. Das, A.K. Guha, Biosorption of chromium by *Termitomyces clypeatus*, Colloids Surf. B 60 (2007) 46–54.
[12] N. Feng, X. Guo, S. Liang, Y. Zhu, J. Liu, Biosorption of heavy metals from aqueous solutions by chemically modified orange peel, J. Hazard. Mater. 185 (2011) 49–54.
[13] D.H.K. Reddy, D.K.V. Ramana, K. Seshaiah, A.V.R. Reddy, Biosorption of Ni(II) from aqueous phase by *Moringa oleifera* bark, a low cost adsorbent, Desalination 268 (2011) 150–157.
[14] J. Buffle, Complexation Reactions in Aqueous Systems: An Analytical Approach, Ellis Horwood, Ltd., Chichester, 1988.
[15] S.K. Papageorgiou, E.P. Kouvelos, E.P. Favvas, A.A. Sapalidis, G.E. Romanos, F.K. Katsaros, Metal–carboxylate interactions in metal–alginate complexes studied with FTIR spectroscopy, Carbohydr. Res. 345 (2010) 469–473.
[16] D.D. Do, Adsorption Analysis: Equilibria and Kinetics, Imperial College Press, London, 1998.
[17] S. Ismadji, S.K. Bhatia, A modified pore-filling isotherm for liquid phase adsorption in activated carbon, Langmuir 17 (2001) 1488–1498.
[18] S. Lagergren, About the theory of so-called adsorption of soluble substances, Kungliga Svenska Vetenskapsakademiens Handlingar 24 (1898) 1–39.
[19] Y.S. Ho, G. McKay, Pseudo-second-order model for sorption processes, Process Biochem. 34 (1999) 451–465.
[20] C.Y. Tan, M. Li, Y.M. Lin, X.Q. Lu, Z.L. Chen, Biosorption of basic orange from aqueous solution onto dried *A. filiculoides* biomass: equilibrium, kinetic and FTIR studies, Desalination 266 (2011) 56–62.
[21] D.L. Guerra, V.L. Leidens, R.R. Viana, C. Airoldi, Application of Brazilian kaolinite clay as adsorbent to removal of U(VI) from aqueous solution: kinetic and thermodynamic of cation-basic interactions, J. Solid State Chem. 183 (2010) 1141–1149.
[22] P.S. Kumar, S. Ramalingam, S.D. Kirupha, A. Murugesan, T. Vidhyadevi, S. Sivanesan, Adsorption behavior of nickel(II) onto cashew nut shell: equilibrium, thermodynamics, kinetics, mechanism and process design, Chem. Eng. J. 167 (2011) 122–131.
[23] A. Bhatnagar, A.K. Minocha, Biosorption optimization of nickel removal from water using *Punica granatum* peel waste, Colloids Surf. B 76 (2010) 544–548.
[24] Y.G. Bermudez, I.L.R. Rico, O.G. Bermudez, E. Guibal, Nickel biosorption using *Gracilaria caudata* and *Sargassum muticum*, Chem. Eng. J. 166 (2011) 122–131.
[25] M.E. Argun, S. Dursun, M. Karatas, Removal of Cd(II), Pb(II), Cu(II) and Ni(II) from water using modified pine bark, Desalination 249 (2009) 519–527.
[26] M.N. Zafar, R. Nadeem, M.A. Hanif, Biosorption of nickel from protonated rice bran, J. Hazard. Mater. 143 (2007) 478–485.
[27] M.Z. Aslam, N. Ramzan, S. Naveed, N. Feroze, Ni(II) removal by biosorption using *Ficus religiosa* (Peepal) leaves, J. Chil. Chem. Soc. 55 (2010) 81–84.
[28] A. Thevannan, R. Mungroo, C.H. Niu, Biosorption of nickel with barley straw, Bioresour. Technol. 101 (2010) 1776–1780.